Kinetic effects in the acceleration of auroral electrons in small scale Alfven waves: A FAST case study

C. C. Chaston,[1] J. W. Bonnell,[1] C. W. Carlson,[1] J. P. McFadden,[1] R. J. Strangeway,[2] and R. E. Ergun[3]

Received 1 July 2002; revised 3 September 2002; accepted 13 September 2002; published 21 March 2003.

[1] In this report we examine the importance of ion and electron kinetic effects in the acceleration of electrons in small scale Alfven waves above the auroral oval. We implement a 1-D two-fluid MHD code approximating the effects of electron inertia and ion and electron temperatures to evaluate their role in accounting for the observed energies of field-aligned electron bursts found in coincidence with these waves above the auroral oval. FAST spacecraft data for a case study event characterized by large auroral ion energies and a hot plasma sheet is employed to define the plasma through which the wave propagates. It is found that strong kinetic effects at altitudes below 5 Earth radii may significantly reduce the amount of electron acceleration possible in the wave in terms of both energy and flux. *INDEX TERMS:* 2704 Magnetospheric Physics: Auroral phenomena (2407); 2712 Magnetospheric Physics: Electric fields (2411); 2752 Magnetospheric Physics: MHD waves and instabilities; 2753 Magnetospheric Physics: Numerical modeling. **Citation:** Chaston, C. C., J. W. Bonnell, C. W. Carlson, J. P. McFadden, R. J. Strangeway, and R. E. Ergun, Kinetic effects in the acceleration of auroral electrons in small scale Alfven waves: A FAST case study, *Geophys. Res. Lett.*, 30(6), 1289, doi:10.1029/2002GL015777, 2003.

1. Introduction

[2] *Hasegawa* [1976] demonstrated that an Alfven wave which propagates through a plasma with $k_\perp \rho_s \approx 1$ or larger (where $k_\perp$ is the wave number, $\rho_s = c_s/\omega_i$ is the ion acoustic gyro-radius with c_s the ion acoustic speed and ω_i the ion gyro-frequency) will carry an electric field parallel to background magnetic field ($\mathbf{B}_0$) and so may accelerate electrons in this direction. On the other hand *Goertz and Boswell* [1979] showed that an Alfven wave with $k_\perp \lambda_e \approx 1$ or larger (where λ_e is the electron inertial length or skin depth) will also carry a parallel electric field. Above the auroral oval in the presence of heated ions both conditions may be met simultaneously for wavelengths projected perpendicular to $\mathbf{B}_0$ ($\lambda_\perp$) of a few kilometers and less. Such waves in an infinite homogeneous plasma approximately obey the dispersion relation,

$$\frac{\omega}{k_\parallel} = V_A \sqrt{\frac{1 + k_\perp^2 \left(\rho_i^2 + \rho_s^2\right)}{1 + k_\perp^2 \lambda_e^2}} \qquad (1)$$

where V_A is the Alfven speed, ω is the wave frequency, $k_\parallel$ is the wave number parallel to $\mathbf{B}_0$ and ρ_i is the ion gyro-radius. This relation is modified from *Lysak and Lotko* [1996] for $k_\perp \rho_i > 1$ as per *Hasegawa* [1976].

[3] Simultaneous observation of heated ions, accelerated electrons, and electric and magnetic field fluctuations satisfying $E_\perp/B_\perp \approx V_A$ above the auroral oval have been documented by *Knudsen and Wahlund* [1998] using observations from the Freja spacecraft. Similar observations have been reported from the from the FAST spacecraft [*Chaston et al.*, 2000] with energies for bulk oxygen that may exceed 100 eV. Based on these observations it is appropriate to assess the role played by kinetic effects in the acceleration of electrons in Alfven waves above the auroral oval.

2. Observations

[4] Figure 1 shows an interval observed from the FAST spacecraft containing Alfvenic activity on the polar cap boundary of the auroral oval near midnight. Panel a) shows the electric field ($E_{\perp 1}$) measured along the spacecraft trajectory (roughly south-north) and perpendicular to $\mathbf{B}_0$ while panel b) shows the wave magnetic field ($B_{\perp 2}$) perpendicular to this direction (roughly west-east) and to $\mathbf{B}_0$. Fourier transform spectra of these fields quantities reveals that $E_{\perp 1}/B_{\perp 2} \approx 2 \times 10^7$ ms^{-1} $\approx V_A$ over the band extending from 0.1 Hz up to the oxygen gyro-frequency at ~15 Hz.

[5] Panels c) and d) show the corresponding electron spectral data. The enhanced electron fluxes are localized around the interval of wave activity. Electron energies shown in c) extend up to several keV and the pitch angle spectra in d) shows that these fluxes are predominately field aligned, with downward (0, 360°), upward (180°) and counter streaming fluxes observed throughout. Moment analysis of the electron distribution averaged over this interval suggests a transverse temperature of 40 eV and a total density of ~50 cm^{-3}. This value is consistent with the density determined from the electron plasma frequency. Nearly all this density is in the accelerated, cool field-aligned electrons below 1 keV.

[6] The remaining panels contain the ion measurements. The peak in energy flux shown in e) above 10 keV corresponds to plasma sheet ions. At energies below 1 keV fluxes of accelerated ionospheric ions are apparent composed in order of increasing energy flux O^+ (panel f), He^+ (panel g) and H^+ (panel h). Panel i) shows show that these ions are distributed close to 90° and 270° suggesting local transverse acceleration. Moment analysis in this case provides an oxygen density of 2 cm^{-3}, an He^+ density of 8 cm^{-3} and an H^+ density of 30 cm^{-3}. The ion plasma sheet component seen by the detector has density less than 1 cm^{-3}. The transverse temperatures of the ion species from the moment analysis over the interval

[1]Space Sciences Laboratory, University of California, Berkeley, California, USA.
[2]Institute for Geophysics and Planetary Physics, University of California, Los Angeles, California, USA.
[3]Laboratory for Atmospheric and Space Physics, University Colorado, Boulder, Colorado, USA.

0094-8276/03/2002GL015777$05.00

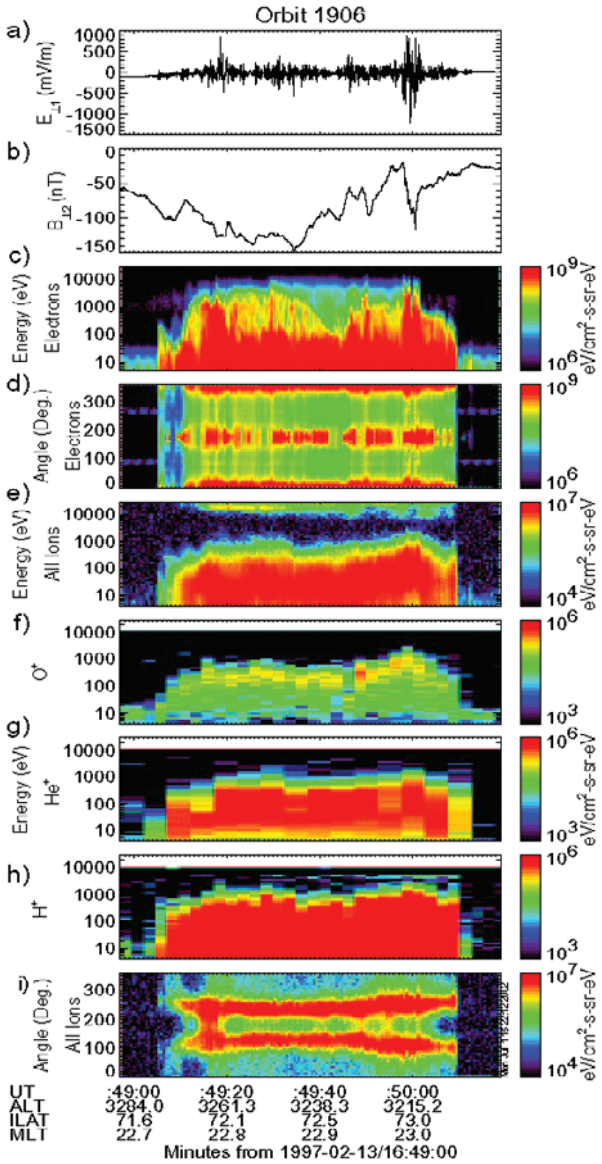

Figure 1. Observations from an active polar cap boundary near midnight. (a) shows the electric field measured perpendicular to $\mathbf{B}_0$ and along the spacecraft trajectory. (b) shows the wave magnetic field perpendicular to $\mathbf{B}_0$ and the spacecraft trajectory. (c) shows the electron energy spectra. (d) shows the electron pitch angle spectra with 0, 360° being downwards and anti-parallel to $\mathbf{B}_0$. (e) shows the total ion energy spectra. (f) shows the O^+ ion energy spectra. (g) shows the He^+ ion energy spectra. (h) shows the H^+ ion energy spectra and (i) shows the total ion pitch angle spectra with 90° and 270° being perpendicular to $\mathbf{B}_0$.

observed are 100., 50., and 40. eV for O^+, He^+ and H^+ respectively.

3. Plasma Model

[7] Figure 2 shows a polar cap boundary plasma model along geomagnetic fieldlines extending from 100 km altitude up to ~5 Re. The densities and temperatures shown in panel a and b for each species have been set to fit the observations at 3260 km discussed above yet are consistent with statistically determined density and composition profiles determined for the polar cap boundary near midnight from FAST observations as indicated by the diamonds. The error bars shown here indicate the range of densities observed at each altitude. We stress that the temperatures used here are appropriate only for an active polar cap boundary. Typical quite time temperatures at altitudes below 1 Re can be expected to be significantly smaller than those given here. The temperature of the oxygen component is modelled in altitude using the same form adopted by *Lysak and Lotko* [1996] as $T_{O+} = 1 + 499 \tanh(\text{altitude} - 100.)/(2\ \text{Re})$ which provides a temperature of 1 eV at 100 km, ~100 eV at 3260 km altitude (as observed) and ~500 eV at altitudes above ~5 Re. For H^+ ions and electrons the profiles are averaged based on the contribution from ionospheric and plasma sheet densities shown in Figure 2a. The ionospheric profiles are given by $T_{H^+,e-} = 1 + 499 \tanh(\text{altitude} - 100.) \times 0.4/(2\ \text{Re})$ and the plasma sheet ion and electron temperatures are taken to be 5 keV and 1 keV respectively consistent with the observations of Figure 1. He^+ ions are not explicitly included and can be expected to have little effect. These parameters provide the phase speeds shown in Figure 2c via Equation 1.

4. Wave Model

[8] The importance of non-zero ion and electron temperatures and finite electron mass along auroral fieldlines in

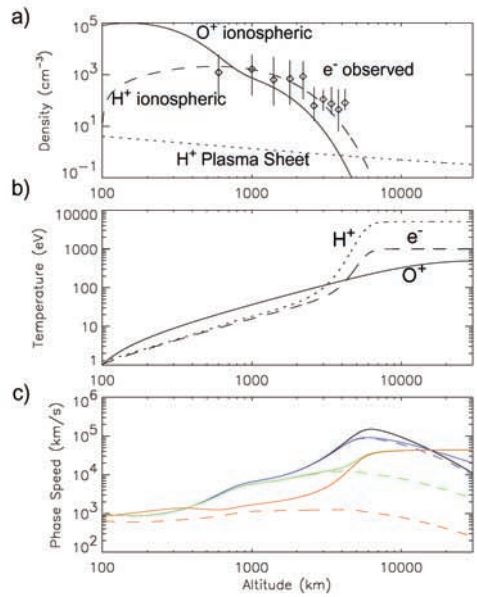

Figure 2. Plasma properties along a fieldline for an active polar cap boundary near midnight. a) shows the density profile of ionospheric H^+ (dashed line) and O^+ (solid line) ions, plasmasheet H^+ ions (dotted line) and statistical observations of electron density (diamonds) with the error bars indicating the range of densities observed in each altitude bin. b) shows the average temperature for O^+ ions (solid line), H^+ ions (dotted line) and electrons (dashed line). c) shows the Alfven speed (solid black line) and phase speeds from Equation 1 for $\lambda_\perp$ in the ionsphere of 10000, 1000, 100 m (solid blue, green and red lines) and phase speeds from Equation 1 in the limit of zero temperature (dashed blue green and red lines).

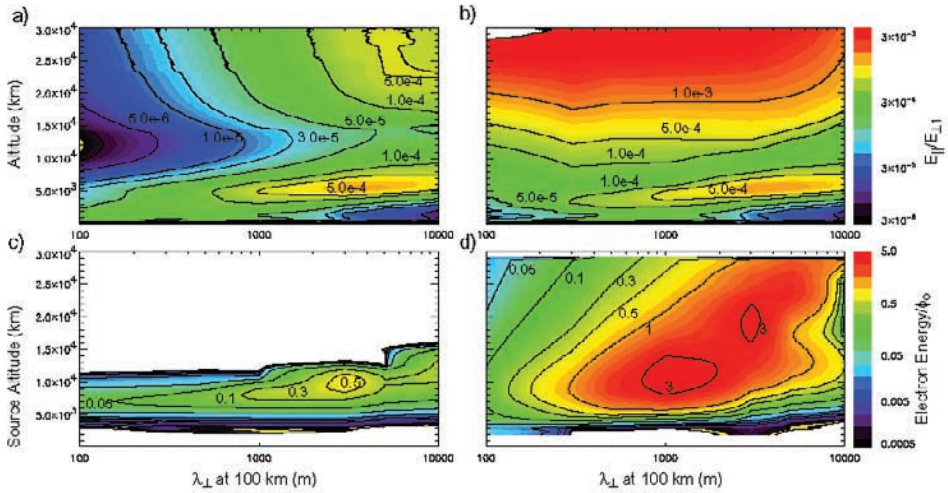

Figure 3. Normalized simulation results. (a) and (b) show the ratio $E_{\parallel}/E_{\perp 1}$ for the kinetic (hot plasma) and purely inertial (cold plasma) cases respectively as functions of $\lambda_{\perp}$ in the ionosphere and altitude. (c) and (d) show the energy gain for a cool electron in the simulated wavefields for the kinetic and purely inertial cases respectively as functions of $\lambda_{\perp}$ and source altitude. These energies are normalised by the amplitude of the applied Gaussian potential ϕ_0 at the magnetospheric end of the simulation required to launch the wave. For $\lambda_{\perp}$ = 10000, 5000, 3000, 1000, 500, 300 and 100m ϕ_0 = 8300, 3900, 2100, 700, 350, 200 and 65 V for the kinetic case and ϕ_0 = 6100, 2100, 1000, 200, 100, 80, and 65 V for the purely inertial case respectively.

modifying the dispersive properties of fieldline resonances has been considered in the linear approximation by *Streltsov et al.* [1998] and in the non-linear case by *Rankin et al.* [1999]. Here to simulate the wavefield of an impulsive kinetic Alfven wave in the simplest manner we Fourier transform the reduced MHD equations from *Streltsov et al.* [1998] in the direction perpendicular to B_o yielding a 1-D model for Alfven waves given by the two coupled differential equations,

$$\frac{V_A^2}{c^2+V_A^2}\left(1+k_{\perp}^2\rho_i^2\right)\frac{\partial A_{\parallel}}{\partial z}+\frac{1\partial\phi}{c\partial t}=0 \tag{2}$$

$$\frac{\left(1+k_{\perp}^2\lambda_e^2\right)}{c}\frac{\partial A_{\parallel}}{\partial t}=\frac{\partial\phi}{\partial z}\left(1+\frac{k_{\perp}^2\rho_s^2}{1+k_{\perp}^2\rho_i^2}\right) \tag{3}$$

where z and t are coordinates along the field aligned direction and in time respectively, and $A_{\parallel}(z, t)$ and $\phi(z, t)$ are the wave vector and scalar potentials respectively. From these potentials the wavefields can be obtained as $E_{\perp 1}(x, z, t) = k_{\perp}\ \phi(z, t)\cos(k_{\perp}x)$ and $B_{\perp 2}(x, z, t) = k_{\perp}A_{\parallel}(z, t)\cos(k_{\perp}x)$. These equations are the two-fluid approximation to the full kinetic treatment appropriate for the altitude range considered. It has been assumed that the plasma properties do not vary appreciably over distances less than one perpendicular wavelength transverse to $\mathbf{B}_0$ which is reasonable given the small transverse scales studied here. The boundary conditions are as given by *Thompson and Lysak* [1996] (hereinafter referred to as T+L).

[9] Differentiating 3 with respect to t and substituting for $\partial\phi/\partial t$ from 2 yields the dispersion relation given by 1. The parallel wave electric field is given by,

$$\begin{aligned}E_{\parallel}&=-\frac{1}{c}\frac{\partial A_{\parallel}}{\partial t}-\frac{\partial\phi}{\partial z}\\&=\frac{1}{c}\frac{\partial A_{\parallel}}{\partial t}\left[\frac{\left(1+k_{\perp}^2\lambda_e^2\right)\left(1+k_{\perp}^2\rho_i^2\right)-\left(1+k_{\perp}^2\left(\rho_i^2+\rho_s^2\right)\right)}{1+k_{\perp}^2\left(\rho_i^2+\rho_s^2\right)}\right]\end{aligned} \tag{4}$$

Using Faraday's law the $\bar{E}_{\perp 1}/\bar{B}_{\perp 2}$ ratio is given by

$$\frac{\bar{E}_{\perp 1}}{\bar{B}_{\perp 2}}=\frac{V_A}{c}\sqrt{\frac{1+k_{\perp}^2\lambda_e^2}{1+k_{\perp}^2\left(\rho_i^2+\rho_s^2\right)}}\left(1+k_{\perp}^2\rho_i^2\right) \tag{5}$$

Using equations 1, 4 and 5 it can be shown that

$$\frac{E_{\parallel}}{E_{\perp 1}}=\frac{k_{\parallel}}{k_{\perp}}\frac{\left(1+k_{\perp}^2\lambda_e^2\right)\left(1+k_{\perp}^2\rho_i^2\right)-\left(1+k_{\perp}^2\left(\rho_i^2+\rho_s^2\right)\right)}{\left(1+k_{\perp}^2\lambda_e^2\right)\left(1+k_{\perp}^2\rho_i^2\right)} \tag{6}$$

[10] These equations reduce to those given by T + L in the inertial case when T_e and $T_i \Rightarrow 0$. However, it should be noted that equations 4 and 6 do not include the imaginary component in $E_{\parallel}$ associated with Landau damping which may become important when $E_{\parallel}$ due to finite $k_{\perp}\rho_s$ becomes comparable with that due to finite $k_{\perp}\lambda_e$.

5. Simulations

[11] Equations 2, 3 are solved for the plasma defined in Figure 2 which is assumed invariant throughout the simulation. This is performed via a leapfrog method as described by T+L and the parallel field determined from equation 4. $k_{\perp}$ scales in altitude with the squareroot of the geomagnetic field which is assumed to vary as $1/r^3$ where r is geocentric distance. This is appropriate only at high latitudes. The time step used is 0.001s. We have assumed Σ_p = 1.0 mho and have launched the wave from the magnetospheric boundary as a Gaussian potential $\phi_0(t)$ with a width of 1 s and a peak magnitude sufficient to provide a maximum amplitude of $E_{\perp 1}$ = 1 V/m. The efficacy of this approach for modelling FAST data has been demonstrated previously by *Chaston et al.* [2002].

[12] Figures 3a and 3b show the maximum $E_{\parallel}$, determined at each altitude and $\lambda_{\perp}$ in the ionosphere from the simulation, normalised by the coincident value of $E_{\perp 1}$. At nearly all altitudes the ratio $E_{\parallel}/E_{\perp 1}$ where inertial effects

alone are considered (3b) is larger than the case including kinetic effects. This follows from Equation 6 where in the cold plasma limit we obtain $E_{\|}/E_{\perp 1} = k_{\|}k_{\perp}\lambda_e{}^2/(1 + k_{\perp}{}^2\lambda_e{}^2)$ while in the limit where $k_{\perp}\ \lambda_e \Rightarrow 0$ we obtain $E_{\|}/E_{\perp 1} = -k\|k_{\perp}\ \rho_s{}^2/(1 + k_{\perp}{}^2\rho_i{}^2)$ and so $E_{\|}$ due to each effect points in the opposite direction and tends to partly cancel. This results in a parallel electric field (for the same $E_{\perp 1}$) several times smaller when kinetic effects are included at altitudes above 10000 km particularly for $\lambda_{\perp}$s in the ionosphere less than 1 km. At altitudes below 10000 km (or the altitude of the peak in the Alfven speed) and $\lambda_{\perp}$ in the ionosphere less than 1 km slightly larger parallel fields are possible in the case including kinetic effects. Equation 6 however does not predict the peak in both a and b between the altitudes 10000 km and 4000 km where much of the incident wave Poynting flux reflects and travels back up the fieldline. During the reflection process over this altitude range the wavefield steepens in the direction parallel to $\mathbf{B}_0$ to provide parallel fields via equation 4 several times larger than predicted from the local approximation. It is here that the strongest $E_{\|}$ is obtained and where multiple keV electron acceleration occurs. The imaginary component in $E_{\|}$, not included in the simulation result shown in 3 a and c, has been calculated in the local approximation from solution of the full electromagnetic dispersion relation [*Davidson*, 1983] and found to be an order of magnitude smaller than the real $E_{\|}$ except at altitudes above 20000 km for $\lambda_{\perp}$ mapped to the ionosphere greater than 5000 km. This defines a rectangular region in the far upper right of Figure 3a where the influence of this component is undetermined and may be significant.

[13] Figures 3c and 3d show the energy gain after reaching the ionosphere for an electron with a field-aligned energy, before interaction with the wave, of 10 eV launched from source altitudes from 2000 to 30000 km. The energies shown are normalized by the peak value of the applied gaussian potential at the magnetospheric end of the simulation and are for a single interaction with the wave, without multiple bounces between wavefronts, or from the magnetic mirror at lower altitudes. The final energy of the electron is rather insensitive to the initial energy, if less than 1 keV but is rather dependent on the position of the electron in the wavefront when $E_{\|}$ maximizes at ~8000 km. These results show that the inclusion of kinetic effects significantly reduces the energy gain possible for an electron over this altitude range. Using the applied potentials detailed in the caption to Figure 3 we find a peak energy of 1 keV in the hot plasma case and 7 keV in the cold plasma case for $\lambda_{\perp}$ in the ionosphere of a few kilometers. Furthermore, in the kinetic case no cold electrons accelerated in the wave reach the ionosphere from above 15000 km altitude since they are unable to achieve resonance with the wave. From Figure 2 the resonant energy required for a cold electron to become resonant with the down going wave above this altitude is ~3 keV. This is an order of magnitude larger than required in the cold plasma case and exceeds the parallel potential drop in the wavefield for perpendicular amplitudes less than the 1 V/m which is an upper limit for observed amplitudes. This will qualitatively lead to smaller wave accelerated electron fluxes at FAST altitudes.

6. Conclusions

[14] Since finite electron inertia and finite ion acoustic gyro-radii effects produce oppositely directed parallel electric fields, the amount of electron acceleration in an Alfven wave possible in a plasma where both effects produce comparable fields is reduced. It has been shown that for an active auroral/polar cap boundary case study the size of the potential in the wavefront may be reduced to less than the energy required for a cool electron to attain resonance with the wave from above an altitude of ~2–3 Re and at least up to the 5 Re limit considered. This may result in significantly lower energies and fluxes for precipitating electrons at the ionosphere relative to the cold plasma case.

[15] **Acknowledgments.** This research was supported by NASA Grant NAG5-3596 and the Physics Department at the Chinese University of Hong Kong.

References

Chaston, C. C., C. W. Carlson, R. E. Ergun, and J. P. McFadden, Alfven waves, density cavities and electron acceleration observed from the FAST spacecraft, *Phys. Scr. T*, *84*, 64, 2000.

Chaston, C. C., J. W. Bonnell, L. M. Peticolas, C. W. Carlson, J. P. McFadden, and R.E. Ergun, Driven Alfven waves and electron acceleration: A FAST case study, *Geophys. Res. Lett.*, *29*(11), 1535, doi:10.1029/2001GL013842, 2002.

Davidson, R. C., Kinetic waves and instabilities in a uniform plasma, in *Basic Plasma Physics*, vol. 1, p. 519, North-Holland, New York, 1983.

Goertz, C. K., and R. W. Boswell, Magnetosphere-ionosphere coupling, *J. Geophys, Res.*, *84*, 7239, 1979.

Hasegawa, A., Particle acceleration by MHD surface wave and formation of aurora, *J. Geophys. Res.*, *81*, 5083, 1976.

Knudsen, D. J., and J. E. Wahlund, Core ion flux bursts within solitary kinetic Alfven waves, *J. Geophys. Res.*, *103*, 4157, 1998.

Lysak, R. L., and W. Lotko, On the kinetic dispersion relation for shear Alfven waves, *J. Geophys. Res.*, *101*, 5085, 1996.

Rankin, R., J. C. Samson, V. T. Tikhonchuk, and I. Voronkov, Auroral density fluctuations on dispersive field line resonance, *J. Geophys. Res.*, *104*, 4399, 1999.

Streltsov, A. V., W. Lotko, J. R. Johnson, and C. Z. Cheng, Small-scale dispersive field line resonances in a hot magnetospheric plasma, *J. Geophys. Res.*, *103*, 26,559, 1998.

Thompson, B. J., and R. L. Lysak, Electron acceleration by inertial Alfven waves, *J. Geophys. Res.*, *101*, 5359, 1996.

J. W. Bonnell, C. W. Carlson, C. C. Chaston, and J. P. McFadden, Space Sciences Laboratory, University of California, Berkeley, CA 94720, USA. (ccc@ssl.berkeley.edu)

R. E. Ergun, Laboratory for Atmospheric and Space Physics, University of Colorado, Boulder, CO 80309, USA. (robert.ergun@colorado.edu)

R. J. Strangeway, Institute for Geophysics and Planetary Physics, University of California, Los Angeles, CA 90024, USA. (strange@igpp.ucla.edu)